https://doi.org/10.31925/farmacia.2024.5.6 **ORIGINAL ARTICLE**

CONTROLLED RELEASE AND ANTIBACTERIAL EFFICACY OF TETRACYCLINE AND METRONIDAZOLE LOADED PCL NANOWIRES ON ZIRCONIUM SUBSTRATE

RAMONA-DANIELA RADU (DUȘMAN) [1], VALENTINA ANUȚA [2]*, ROBERTA IRODIA [1], GEORGETA TOTEA [3], DOINA DRAGĂNESCU [4], IOANA DEMETRESCU [1,5]

[1]*Department of General Chemistry, Faculty of Chemical Engineering and Biotechnologies, National University of Science and Technology POLITEHNICA Bucharest, 313 Splaiul Independenței, 060042, Bucharest, Romania*
[2]*Department of Physical and Colloidal Chemistry, "Carol Davila" University of Medicine and Pharmacy, 020956, Bucharest, Romania*
[3]*Buftea Obstetrics and Gynaecology Hospital, 070000, Ilfov, Romania*
[4]*Department of Pharmaceutical Physics and Informatics, "Carol Davila" University of Medicine and Pharmacy, 020956, Bucharest, Romania*
[5]*Academy of Romanian Scientists, 3 Ilfov Street, 050044, Bucharest, Romania*

**corresponding author: valentina.anuta@umfcd.ro*

Manuscript received: June 2024

Abstract

This study investigates the controlled release and antibacterial efficacy of tetracycline and metronidazole loaded on polycaprolactone (PCL) nanowires deposited on zirconium (Zr) substrate. The integration of PCL nanowires on Zr substrate offers a novel approach in enhancing the therapeutic effects of antibiotics, particularly against antibiotic-resistant strains. The PCL nanowires serve as an efficient drug delivery system, providing sustained and targeted release of the antibiotics, thereby maintaining therapeutic concentrations at the site of infection. The antibacterial activity of these nanowire-coated substrate was assessed against *Escherichia coli* and *Staphylococcus aureus*, demonstrating significant inhibition of bacterial growth. The study highlights the potential of this nanotechnology-based system in improving the efficacy of antimicrobial therapies, especially in the context of medical implants and wound healing.

Rezumat

Acest studiu investighează eliberarea controlată și eficacitatea antibacteriană a tetraciclinei, respectiv metronidazolului înglobate în nanofibre de policaprolactonă (PCL) depuse pe substrat de zirconiu (Zr). Înglobarea antibioticelor în nanofibre de PCL depuse pe substrat de Zr oferă o abordare nouă pentru îmbunătățirea efectului terapeutic al antibioticelor, în special împotriva tulpinilor rezistente la antibiotice. Nanofibrele de PCL servesc ca un sistem eficient de cedare a medicamentelor, oferind eliberare susținută și țintită a antibioticelor, menținând astfel concentrațiile terapeutice la locul infecției. Activitatea antibacteriană a acestor antibiotice înglobate în nanofibre a fost evaluată împotriva *Escherichia coli* și *Staphylococcus aureus*, demonstrând o inhibare semnificativă a creșterii bacteriene. Studiul evidențiază potențialul acestui sistem de cedare bazat pe nanotehnologie de a îmbunătăți eficacitatea terapiilor antimicrobiene, în special în contextul implanturilor medicale și al vindecării rănilor.

Keywords: nanowires, antibiotics, drug delivery system

Introduction

The rapidly growing area of nanotechnology has heralded a new era in biomedical applications, particularly in the realm of drug delivery systems [1-3]. One notable innovation is the use of nanowires on zirconium substrate to facilitate the controlled release of antibiotics such as tetracycline and metronidazole [4-7].

The persistent challenge of managing bacterial infections, particularly those caused by antibiotic-resistant strains, necessitates the development of advanced drug delivery systems that can enhance therapeutic efficacy and reduce side effects [8-10]. Traditional antibiotic therapies often suffer from issues such as poor bioavailability, rapid drug degradation and systemic toxicity, which can be mitigated by innovative approaches like nanotechnology-based drug delivery systems [11, 12]. In this context, the use of nanowires on zirconium substrate has emerged as a promising strategy for the controlled release of antibiotics, including tetracycline and metronidazole, offering significant advantages in terms of targeted delivery and sustained antibacterial effects [13-15].

Zirconium is widely recognised for its exceptional biocompatibility, corrosion resistance and mechanical strength, making it a suitable material for biomedical applications such as implants and prosthetics [16-18].

Also, it can inhibit the growth of microorganisms [19-22]. The smooth and dense surface of zirconium can reduce bacterial adhesion and biofilm formation [19, 20]. The integration of drug-loaded nanowires on zirconium substrate can transform these materials into potent antibacterial platforms [23]. The high surface area of nanowires allows for a greater loading capacity of antibiotics, facilitating a higher local concentration of the drug at the infection site and thus enhancing its therapeutic efficacy and reducing systemic side effects [23-26]. To enhance the well-known antibacterial effect of zirconium, researchers have explored the incorporation of various antibiotics to create more potent antimicrobial materials [9, 21]. Among these antibiotics, tetracycline and metronidazole stand out due to their strong antibacterial properties [27-30]. However, while tetracycline, is a broad-spectrum antibiotic widely used to treat various bacterial infections, its effectiveness can be compromised by rapid degradation and resistance mechanisms [27-28]. Tetracycline inhibits protein synthesis in bacteria by binding to the 30S ribosomal subunit. It is effective against a wide range of bacteria, including both gram-positive and gram-negative organisms [27]. Similarly, metronidazole, effective against anaerobic bacteria and protozoa, often requires precise delivery to maintain its therapeutic levels and minimize side effects [29, 30]. Metronidazole is a prodrug that requires activation within the microbial cell. It undergoes reduction by nitroreductase enzymes, which are present in anaerobic bacteria and certain protozoa. This reduction converts metronidazole into its active form, which can then interact with cellular components. The reduced form of metronidazole generates reactive intermediates, such as nitroso radicals and other free radicals. These highly reactive molecules can damage cellular macromolecules. The reactive intermediates produced from metronidazole primarily target DNA. They cause strand breaks and cross-linking of DNA, which interferes with DNA replication and transcription. This DNA damage leads to the inhibition of nucleic acid synthesis and eventually causes cell death [31]. Tetracycline and metronidazole effectiveness is often limited by the inability to maintain therapeutic concentrations at the site of infection and is hampered by factors such as poor solubility, rapid degradation and limited penetration into bacterial biofilms [8, 32]. Embedding these antibiotics in nanowires on zirconium substrate addresses these challenges by providing a controlled, sustained and targeted release of these antibiotics, thereby maintaining their antibacterial activity over a prolonged period [33, 34]. This sustained release mechanism not only enhances the efficacy of the antibiotics but also minimizes the risk of resistance development by maintaining therapeutic drug levels and reducing the need for frequent dosing [35].

Nanostructures significantly enhance surfaces, with nanowires being particularly advantageous as drug delivery systems. Their high surface area-to-volume ratio and porous structure make nanowires ideal for loading and controlling the release of therapeutic agents, such as drugs (*e.g.* antibiotics), proteins and growth factors [36]. Studies have demonstrated that the nanowire structures not only serve as effective carriers for antibiotics, but also exhibit intrinsic antibacterial properties due to their unique physical and chemical characteristics [37, 38]. The synergy between the controlled drug release from the nanowires and the inherent properties of the zirconium substrate creates a potent antibacterial system that can address various types of bacterial infections, including those caused by drug-resistant strains [39, 40]. Moreover, the physical structure of nanowires, such as their nanoscale dimensions, high surface area-to-volume ratio that allows for a greater loading capacity of antibiotics and surface roughness, can disrupt bacterial cell membranes and inhibit biofilm formation [8], which is a common defence mechanism of bacteria against antibiotics [36, 41, 42]. Additionally, the nanoscale interactions between the nanowires and bacterial cells can enhance the penetration of the antibiotics into the bacterial cells, further boosting their antibacterial efficacy [39].

Recent studies have demonstrated the potential of antibiotic-loaded nanowires on zirconium substrate in various biomedical applications [43, 44]. For instance, a study on tetracycline-loaded titanium dioxide nanowires on zirconium substrate showed significant antibacterial activity against both Gram-positive and Gram-negative bacteria, highlighting the broad-spectrum applicability of this approach [45]. Similarly, metronidazole loaded on nanowires have shown promising results in preventing infections associated with surgical implants and other medical devices, thereby reducing the incidence of implant-related complications [46-48].

The combination of controlled drug release and the inherent antibacterial properties of nanowires provides a dual mechanism of action that is highly effective in combating bacterial infections [43, 47]. This dual approach is particularly important in the context of multidrug-resistant bacteria, where traditional antibiotics alone may be insufficient to eradicate the infection [49]. By ensuring a sustained release of antibiotics and simultaneously exerting mechanical disruption on bacterial cells, nanowire-based delivery systems on zirconium substrate represent a significant advancement in the field of antimicrobial therapy [43].

In conclusion, the use of nanowires on zirconium substrate for the controlled release of antibiotics such as tetracycline and metronidazole hold great promise in enhancing antibacterial efficacy and overcoming the limitations of conventional antibiotic therapies [5, 15, 30, 46]. The synergy between the high drug

loading capacity, sustained release and the inherent antibacterial properties of nanowires creates a potent platform for the treatment of bacterial infections, particularly those caused by resistant strains, which is particularly crucial in medical implants and wound healing applications [33, 34, 50]. The incorporation of nanotechnology in this manner offers a novel method to address persistent infections, particularly in medical devices where bacterial colonization can lead to severe complications [50].

Further research and development in this area are essential to further refine these technologies and translate them into clinical practice, ultimately improving patient outcomes and addressing the growing challenge of antibiotic resistance.

Materials and Methods

Reagents

Zirconium (Zr) and polycaprolactone (PCL) granules were procured from Sigma Aldrich, USA. For the preparation of the polymer solution, chloroform ($CHCl_3$) from Carl Roth, Germany and N,N-dimethylformamide (DMF) from Alfa-Aesar, USA, were used. Chloroform acted as a primary solvent for dissolving the PCL, while DMF was added to adjust the viscosity and electrical conductivity of the solution, optimizing it for the electrospinning process.

Phosphate Buffered Saline (PBS) with a pH of 7.4 was prepared to maintain physiological conditions during experiments, using analytical reagent grade salts sourced from Sigma Aldrich, USA, dissolved in ultrapure water with a resistivity of 18.2 $M\Omega \cdot cm^{-1}$ obtained from a Milli-Q EQ 7008 water purification system (Merck Millipore, Burlington, MA, USA). This high-purity water ensured the absence of contaminants that could interfere with experimental results.

Tetracycline hydrochloride ($C_{22}H_{24}N_2O_8 \cdot HCl$) and metronidazol ($C_6H_9N_3O_3$) were provided by Guinama Biesterfeld international Gmbh (Hamburg, Germany). Two reference strains, *Escherichia coli* (ATCC 25922) and *Staphylococcus aureus* (ATCC 25923), were used to assess antimicrobial activity.

Equipments and methods

The electrospinning process was conducted using a high-voltage power source (PS/EJ30P20, Glassman High Voltage, Inc., High Bridge, NJ, USA) and a Legato 180 syringe pump (KD Scientific, Holliston, MA, USA) to ensure consistent and controlled nano-fibre production. The high-voltage power source was employed to generate the necessary electric field for electrospinning. The pump was used to deliver the polymer solution at a precise and constant flow rate. The Legato 180 pump is renowned for its accuracy and reliability, which are vital for maintaining a steady supply of the solution to the electrospinning needle. This steady flow rate is essential for achieving consistent fibre diameter and morphology.

In order to investigate the surface morphology, scanning electron microscopy (SEM) was conducted using a Hitachi TM4000 plus scanning electron microscope equipped with Energy Dispersive X-ray (EDX) Oxford detector for chemical analysis alongside imaging (HITACHI High-Technologies Corp. (Tokyo, Japan)). For the analysis, the samples were carefully positioned on a conductive copper sticker. This conductive adhesive ensures proper grounding and enhancing image quality. Once secured, the samples were introduced into the SEM chamber and analysed directly, allowing for high-resolution imaging. The sample was examined under low-vacuum mode to reduce the need for extensive sample preparation and to prevent charging of non-conductive materials. Accelerating voltages of 10 to 15 kV were applied, which were deemed optimal for balancing resolution and minimizing sample damage. Both secondary electron (SE) and backscattered electron (BSE) detection mode was used for imaging, providing detailed topographical information of the sample surface. This setup allowed for high-quality imaging while preserving the integrity of the sample.

The Energy Dispersive X-ray Spectroscopy (EDX) analysis is a technique used to determine the elemental composition of the sample. X-Axis (Energy in keV) represents the energy levels of the X-rays emitted by the elements present in the specimen. The peaks correspond to specific elements based on their characteristic X-ray energies. Y-Axis (Counts *per* second *per* electron volt, cps/eV) indicates the intensity of the detected X-rays, which is proportional to the concentration of the respective elements in the sample.

Fourier-transform infrared spectroscopy (FT-IR) was performed to identify the chemical structure of the coated samples. The analysis was carried out using a Perkin-Elmer Spectrum 100 spectrometer (Perkin-Elmer, Shelton, CT, USA) in transmittance mode. The FT-IR spectra were recorded over a wavenumber range from 500 to 4000 cm^{-1}. This range covers the key regions where most functional groups absorb infrared light, allowing for comprehensive analysis of the sample's chemical structure.

The contact angle measurement was performed to determine the wettability of the surface of the samples. The measurements were carried out using a KSV Instruments CAM100 contact angle meter (Espoo, Finland). This instrument is designed to precisely measure the contact angle formed between a liquid droplet and a solid surface. The samples to be analysed were positioned securely on the stage of the contact angle meter. A 5 µL droplet of distilled water was carefully dispensed onto the surface of the sample. Measurements were taken at three different areas on the surface of each sample. Using image analysis software, the contact angle formed between the water droplet and the sample surface was measured. The contact angles from the three different areas were recorded. The average contact angle was then calculated

to provide a single representative value for the sample's surface wettability.

In vitro release tests were conducted using a Vision G2 Classic 6 Dissolution Tester (Teledyne Hanson, Chatsworth, CA, USA) to evaluate the release profile of tetracycline and metronidazole. The tests utilised small-volume flat-bottom 150 mL vessels and a mini-paddle assembly, operating at a stirring speed of 50 rpm. The selection of these vessels and the mini-paddle configuration was based on their ability to simulate the dissolution environment accurately and provide uniform mixing, essential for reliable and reproducible results. The samples were immersed in 100 mL PBS, maintained at a controlled temperature (37°C), replicating physiological conditions. Sodium azide (0.02%, w/v) was added to inhibit bacterial growth during the test. The stirring speed of 50 rpm was chosen to ensure consistent agitation, which is crucial for maintaining homogeneity in the dissolution medium and for the accurate measurement of the release rates of the drugs. To quantify the amount of tetracycline and metronidazole released during the tests, samples were analysed using a Jasco LC-4000 Series HPLC system (JASCO Corporation, Tokyo, Japan). Samples were periodically withdrawn from the dissolution medium at predefined time intervals, filtered and injected into the HPLC system for analysis. High-performance liquid chromatography (HPLC) was selected for its high sensitivity and specificity in detecting and measuring tetracycline and metronidazole concentrations. This method ensured precise quantification, allowing for a detailed understanding of the release kinetics and the overall efficiency of the drug delivery system.

To investigate the drug release mechanism, the release data were fitted to various mathematical models describing different kinetic processes. These models included zero order, first order, Higuchi, Hixson-Crowell, Korsmeyer-Peppas and Weibull equations, each representing a distinct release pattern based on diffusion or other underlying mechanisms [51].

To evaluate antimicrobial efficacy, *Escherichia coli* (ATCC 25922) and *Staphylococcus aureus* (ATCC 25923) were cultured on Columbia Agar with 5% sheep blood (Graso Biotech) and incubated for 24 hours at 37°C in an Incudigit-TFT incubator (JP SELECTA). The inoculum was prepared in physiological saline, adjusted to 0.5 McFarland units using a Den-1 densitometer (Biosan) and spread on Mueller-Hinton agar plates (Graso Biotech).

Substrate Coating Protocol

Deposition of PCL nanofibers on Zr Samples. The process of preparing and modifying Zr samples with PCL nanofibers involved several steps to ensure uniform and effective coating (Figure 1).

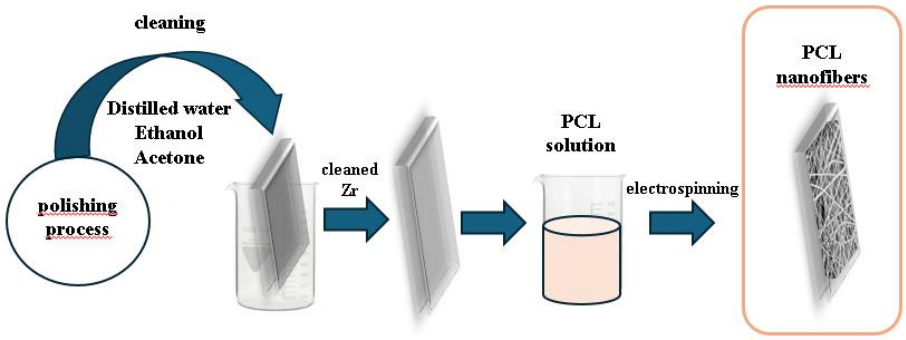

Figure 1.
An effective scheme for obtaining PCL nanofibers

Sample Preparation: Zr samples, measuring 25 mm × 25 mm × 1 mm, underwent a polishing process using silicon carbide (SiC) paper with increasing grit sizes ranging from P320 to P1200. This step was crucial for achieving a smooth surface necessary for uniform nanofiber deposition.

Cleaning Procedure: After polishing, the Zr samples were cleaned to remove any contaminants. They were sequentially immersed in an ultrasonic bath containing distilled water, ethanol and acetone for 10 minutes each. This thorough cleaning process ensured the removal of any residual polishing debris or organic contaminants from the surface of the samples.

Preparation of PCL Solution: A PCL solution was prepared by dissolving 0.4 g of PCL granules in a mixture of 3.6 mL chloroform ($CHCl_3$) and 0.4 mL N,N-dimethylformamide (DMF). This solution was stirred magnetically for 15 minutes to ensure complete dissolution of the PCL granules. Subsequently, it underwent 10 minutes of ultrasonication to achieve homogenization and to eliminate air bubbles, ensuring a smooth and uniform solution suitable for electro-spinning.

Electrospinning Process: The electrospinning setup involved transferring the prepared PCL solution into a 1 mL plastic syringe, which was connected to a pumping system set to deliver the solution at a constant flow rate of 0.5 mL/h. The syringe needle was positioned approximately 10 cm from the Zr

samples, which were fixed onto a copper collector plate covered with aluminium foil.

Deposition of PCL nanofibers: The electrospinning process commenced by applying a high voltage of 15 kV from a power source to the syringe needle. The electric field generated by this voltage caused the PCL solution to form a fine jet that was drawn towards the grounded Zr samples. The distance between the needle tip and the sample surface was maintained at 10 cm to facilitate the formation of nanofibers.

Duration of Deposition: The electrospinning process continued for a total duration of 60 minutes, during which time the PCL fibbers gradually accumulated on the surface of the Zr samples. This duration was optimised to achieve a desired thickness and density of PCL nanofibers on the Zr substrate.

Preparation of PBS Solution. The PBS (Phosphate Buffered Saline) solution used in this study was prepared following the protocol established in a previous work [52]. This solution served as a standardised medium for characterizing both the uncoated Zr samples and the Zr samples coated with PCL nanofibers (Zr-PCL).

Drug loading and release

The process of drug loading and release from Zr-PCL nanofiber samples involved several steps to ensure accurate characterization and analysis:

Preparation of Drug Solutions. Tetracycline Solution: Zr-PCL nanofiber samples were immersed in a 10 mL solution containing 5 g/L tetracycline and kept for 24 hours. Metronidazole Solution: Similarly, another set of Zr-PCL nanofiber samples were immersed in a 10 mL solution containing 5 g/L metronidazole and kept for 24 hours. This step allowed for the adsorption/ loading of the drugs into the PCL nanofiber matrix.

HPLC Analysis. Quantitative analysis of the drugs was performed using a Jasco LC-4000 Series HPLC system (Jasco Corp., Tokyo, Japan). The HPLC system included a PU-4180 quaternary pump, CO-4061 column thermostat, AS-4150 autosampler and MD-4010 diode array detector. A Kinetex EVO C18 Core Shell column with 2.6 μm particle size (Phenomenex Inc., Torrance, CA, USA) was used for separation, maintained at 45°C. A 10 μL injection volume of the filtered samples was injected into the HPLC system. The mobile phase consisted of 0.1% formic acid and acetonitrile in an 88:12 (v/v) ratio, delivered at a flow rate of 0.7 mL/min. Calibration curves for both drugs were constructed in the 0.1 - 10 μg/mL range. Detection and quantification of tetracycline and metronidazole were performed at 357 nm [53] and 320 nm [54], respectively.

Drug Loading: The drug-loaded, polymer-coated Zr plates were immersed in 5 mL of dioxane and subjected to vortex mixing for 2 minutes. This process ensured the dissolution of both the drug and the polymer. 100 μL of the resulting solution was accurately transferred and diluted to 1 mL using the mobile phase specific to the HPLC method. The diluted solution was then centrifuged at 15,000 rpm for 10 minutes to remove any undissolved particulates and analysed by HPLC.

Drug Release Studies. The release of tetracycline and metronidazole from the PCL nanofiber coatings was evaluated by immersing the coated Zr plates, fixed on aluminium stubs, into small-volume dissolution vessels. The coated side of the samples was exposed to 100 mL of phosphate buffered saline (PBS), which simulates physiological conditions. Aliquots of 1.5 ± 0.1 mL were withdrawn at predetermined time intervals up to 360 hours and immediately replaced with an equal volume of fresh PBS at the same temperature. The withdrawn samples were filtered using a 0.45 μm RC syringe filter (Phenomenex Inc., Aschaffenburg, Germany) to remove any particulates or fibres. The concentrations of tetracycline and metronidazole in the filtered samples were quantitatively analysed by HPLC.

Experimental Replication: All experiments were conducted in triplicate to ensure reliability and reproducibility of the results.

Antibacterial effect

The procedure to test the antimicrobial activity is described below.

Cultivation of Bacterial Strains. Strain Selection: We chose *Escherichia coli* (ATCC 25922) and *Staphylococcus aureus* (ATCC 25923) as the reference strains for this study. These strains are commonly used as standard controls in antimicrobial susceptibility testing due to their well-characterised responses to various antibiotics. Growth Conditions: The strains were grown on Columbia Agar plates enriched with 5% sheep blood, which supports the growth of a wide range of bacteria, including those that require additional nutrients provided by blood. This medium also allows for the visualization of haemolysis, which can be useful in differentiating bacterial species. Incubation: The inoculated plates were incubated for 24 hours at 37°C in an Incudigit-TFT incubator. The controlled temperature and time are crucial to ensure optimal bacterial growth and the development of well-defined colonies.

Preparation of the Inoculum. Colony Selection: After incubation, 2 - 3 well-isolated colonies from each plate were selected for further testing. The colonies were chosen based on their typical morphology, ensuring that they represent the target bacteria. Inoculum Preparation: The selected colonies were transferred to a tube containing physiological saline. This step involves suspending the bacterial cells in a sterile solution to create a homogenous bacterial suspension. Turbidity Adjustment: The bacterial suspension was adjusted to 0.5 McFarland units using a Den-1 densitometer. The 0.5 McFarland standard corresponds to an approximate bacterial concentration of 1.5×10^8 colony-forming units (CFU) *per* millilitre. Accurate adjustment of the inoculum is critical for reproducibility and reliability in susceptibility testing.

Antimicrobial Susceptibility Testing. Plate Preparation: The adjusted inoculum was spread onto Mueller-Hinton agar plates. Mueller-Hinton agar is the standard medium used for antibiotic susceptibility testing because it provides a consistent environment that allows for the proper diffusion of antibiotics. Inoculation: The plates were then inoculated with the bacterial suspension using a sterile swab, ensuring uniform distribution across the entire surface of the agar. This step is vital to ensure that any observed zones of inhibition around the antibiotic samples reflect the true susceptibility of the bacteria.

Follow-Up Steps. Application of Antibiotic Discs: After inoculating the Mueller-Hinton plates, samples containing antibiotics, such as tetracycline or metronidazole, embedded in nanofibers, were placed in the centre of the agar surface. This setup facilitates the assessment of the drug delivery systems. Incubation: The plates were then incubated at 37°C for 24 hours, providing sufficient time for the antibiotics to diffuse through the agar and interact with the bacteria. During incubation, two phenomena occur at the same time: the diffusion of antibiotics in the culture medium and bacterial growth, thus resulting in the appearance of a visible halo on the plate if there is sensitivity to the selected antibiotic. Assessment of Results: After incubation, the plates were examined for zones of inhibition around each disc. These zones indicate the effectiveness of the antibiotics against the bacterial strains.

Results and Discussion

Sample morphology characterization (SEM)

The morphology of the unloaded PCL nanofibers is presented in Figure 2a. The higher magnification (1000x) provides a close-up view with a detailed perspective of the nanofiber dimensions and their spatial arrangement and reveals the intricate details of the PCL nanofibres on the zirconium substrate (Figure 2 (a)). The nanofibers are shown as fine, thread-like structures, densely packed and forming a highly porous network.

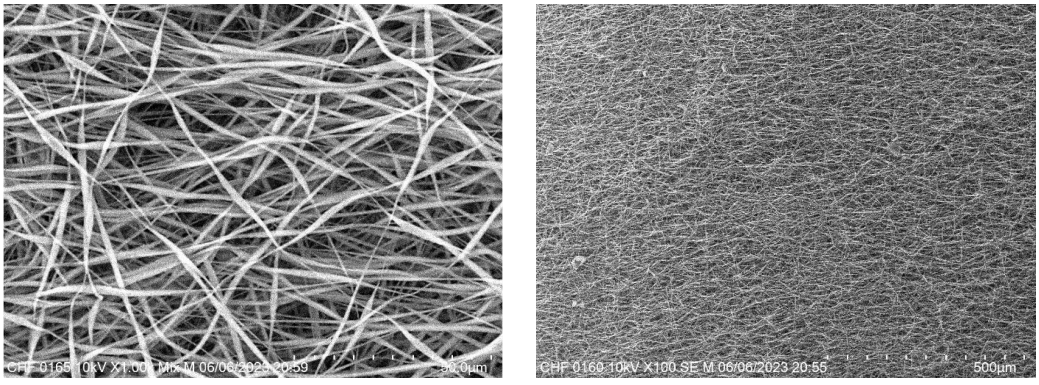

(a) (b)

Figure 2.
SEM Micrographs of PCL Nanofibers on Zirconium Substrate at different magnifications at (a) 1000x magnification and (b) 100x magnification

The uniformity in the diameter of the nanofibers is evident, with the fibres appearing smooth and continuous. This high magnification highlights the fibre alignment and the small pore sizes within the network, which are critical for applications requiring precise control over fibre morphology and porosity, such as in biomedical scaffolds or controlled drug release systems. Figure 2b showcases a broad, uniform coverage of PCL nanofibers. The PCL nanofibers form a compact, interwoven network that spans the entire visible area, creating a non-woven mat. The fibres appear consistently thin and well-distributed, with no visible defects or irregularities.

SEM analysis shows the morphology of the PCL Nanofibers Loaded with Metronidazole on Zirconium (Zr-PCL-MTZ). Therefore, in the Figure 3a, the image was acquired at a magnification of 1000x. The scale bar at the bottom right of the image indicates a length of 50 micrometres, providing a reference for the size and density of the nanofibers. The nanofibers form a dense, non-woven mat with a high surface area, which is beneficial for applications like controlled drug release, where surface interactions are critical. The nanofibers appear to have a consistent diameter, ranging from nanometres to a few micrometres. The fibres are randomly oriented, forming a highly porous network that can facilitate fluid penetration and drug diffusion. The high-resolution nature of the SEM image allows for detailed observation of the fibre surfaces, which appear smooth, indicating a successful electrospinning process with uniform polymer dissolution and drug incorporation. Further, Metronidazole is uniformly embedded within the PCL nanofibers and it seems that zirconium substrate provides a stable and biocompatible base for the nanofibers.

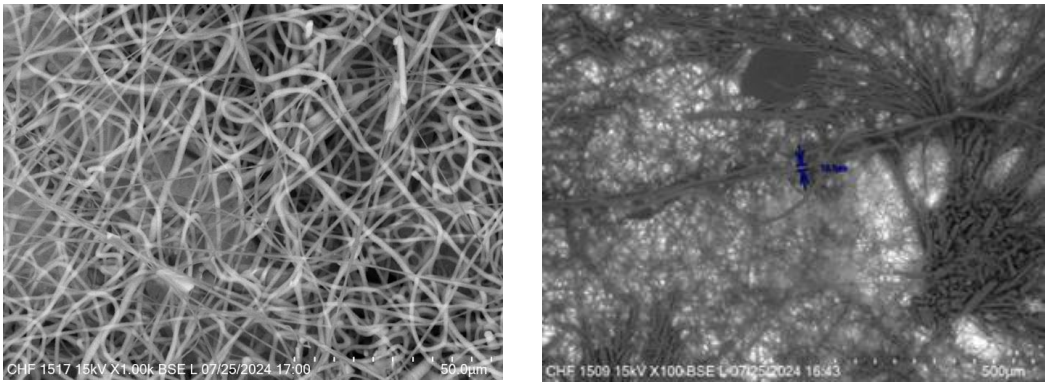

(a) (b)

Figure 3.
SEM Micrographs of PCL Nanofibers Loaded with Metronidazole on Zirconium Substrate at (a) 1000x magnification and (b) 100x magnification

For Figure 3b the lower magnification image (100x) shows the overall arrangement and distribution of the PCL nanofibers on the substrate. The image shows areas where fibres are densely packed, as well as regions where they form aggregates or clusters. These features could indicate zones of enhanced mechanical strength or areas where drug release might be more concentrated. The image highlights the extensive porosity of the nanofiber mat.

Figure 4a shows a dense and intricate network of PCL nanofibers, which have been loaded with tetracycline. The nanofibers, appearing as thin, thread-like structures, are intricately interlaced, creating a non-woven mat. The image emphasizes the uniform diameter of the nanofibers, which together form a highly porous and interconnected web.

The nanofibers' high surface area-to-volume ratio is evident, which is beneficial for drug delivery applications. The tetracycline is embedded within these nanofibers. The backscattered electron (BSE) imaging mode used here helps in distinguishing the fibres from the background, providing a clear contrast.

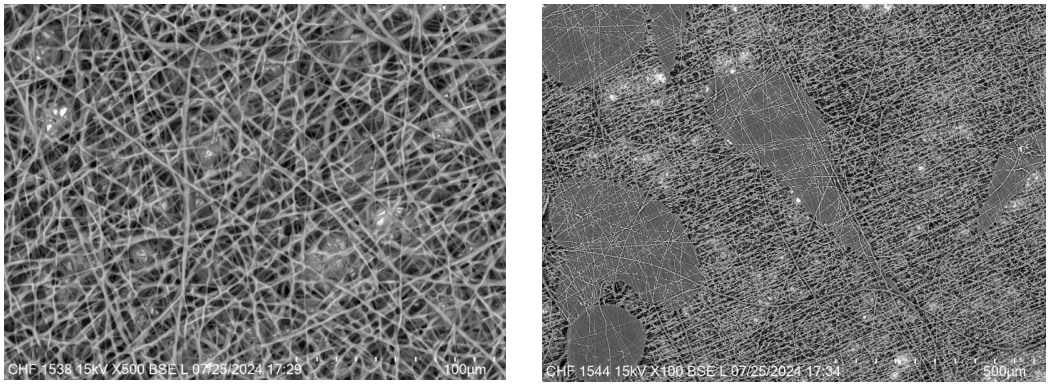

(a) (b)

Figure 4.
SEM Micrographs of PCL Nanofibers Loaded with Tetracycline on Zirconium Substrate at (a) 500x magnification and (b) 100x magnification

Figure 4b presents a SEM image at a lower magnification of 100x and it offers a wider view of the PCL nanofibres containing tetracycline on the zirconium substrate. At this magnification, the image shows a broader coverage of the nanofiber mat, illustrating the distribution and adherence of the fibres across the substrate. It can be observed that there are flat regions which are likely the exposed areas of the zirconium substrate. These areas appear darker in contrast due to the BSE imaging mode, which enhances the visibility of the nanofibers overlaying these regions. The nanofibers maintain a consistent morphology and distribution across the substrate, indicating a uniform coating process.

Additionally, Figure 4b captures some bright spots that might represent clusters or aggregates of tetracycline within the nanofiber network.

SEM images of the synthesized PCL nanowires reveal a consistent and precise morphology, which plays a crucial role in their antimicrobial effectiveness. The results suggest that these nanowires are highly effective in microbial activity inhibition, making them promising candidates for antimicrobial applications.

EDX Analysis

Figure 5 presents the Energy Dispersive X-ray (EDX) spectrum of metronidazole-loaded PCL nanofibers, offering a detailed examination of the elemental composition. The spectrum displays significant peaks corresponding to carbon (C) at approximately 0.3 keV and oxygen (O) around 0.5 keV, which are key constituents of both the PCL matrix and metronidazole. Additionally, peaks near 4.5 keV and 4.9 keV indicate the presence of titanium (Ti), attributed to the zirconium substrate, which can contain Ti as an alloying element. The weight percentages and standard deviations for each element are: Oxygen (O): 34.4 wt% ($\sigma = 0.1$), Carbon (C): 31.7 wt% ($\sigma = 0.1$), Titanium (Ti): 33.9 wt% ($\sigma = 0.0$). The weight percentages indicate the relative abundance of each element in the sample. The standard deviation values suggest high precision in the measurements, implying a very consistent detection of this element. The significant presence of carbon is indicative of the PCL matrix, as PCL is composed of carbon atoms in its polymer backbone. Metronidazole also contributes to the carbon content due to its organic nature. The oxygen peak is consistent with both the PCL polymer and metronidazole. PCL contains ester linkages (-CO-O-) contributing to the oxygen content. Metronidazole contains nitro (NO_2) and hydroxyl (OH) groups, both of which contain oxygen. Despite nitrogen (N) being a component of metronidazol, it is not explicitly shown in the spectrum provided, because the nitrogen peak may overlap with other peaks or background noise, making it difficult to resolve. The elemental analysis shows deviations from the theoretical composition of pure PCL (66.67% C and 26.67%), particularly in the oxygen and carbon content. The higher oxygen percentage and lower carbon percentage align with the presence of metronidazole, which has a lower carbon content relative to PCL but contains additional oxygen atoms as part of its molecular structure (*e.g.*, in its nitro group (-NO2) and hydroxyl group (-OH)). These shifts in elemental composition are consistent with the chemical structure of metronidazole, confirming its successful incorporation into the PCL matrix.

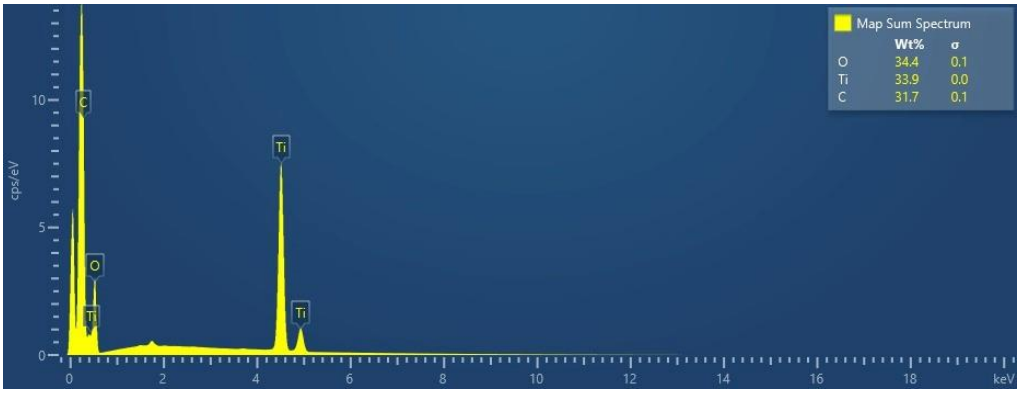

Figure 5.
EDX Spectrum Analysis of Metronidazole loaded on PCL Nanofibers

The EDX spectrum analysis confirms the presence of carbon and oxygen, which are consistent with the composition of metronidazole-loaded PCL nanofibers. The analysis supports the successful incorporation of metronidazole into the PCL nanofibers and provides a detailed elemental composition of the sample.

The EDX spectrum provides a quantitative analysis, identifying which elements are present in the sample and their proportions. The elemental mapping (Figure 6) gives a visual representation of where these elements are distributed across the sample. This figure is a layered elemental map obtained through energy-dispersive X-ray spectroscopy (EDS) overlaid on the SEM image.

The maps complement the EDX spectrum by showing how elements are distributed spatially, rather than just providing an average composition.

The blue map (Ti Kα1) shows the distribution of titanium in the sample. The relatively low intensity, or scattered appearance of the blue regions suggests that Ti is present in lower concentrations. The fact that Ti does not appear uniformly across the entire map implies that it serves as a foundation rather than being integrated into the nanowires themselves.

The red map (C Kα1_2) shows the distribution of carbon, which is the main element in both PCL and metronidazole. The dense and uniform red regions indicate that carbon is widely and uniformly distributed across the nanowires, which is expected given that PCL is an organic polymer and would form the bulk of the nanowires.

The green map (O Kα1) shows the distribution of oxygen in the sample. Oxygen is present both in PCL and possibly in metronidazole. The green regions suggest that oxygen is also evenly distributed, consistent with the PCL structure, which contains oxygen atoms in its ester linkages.

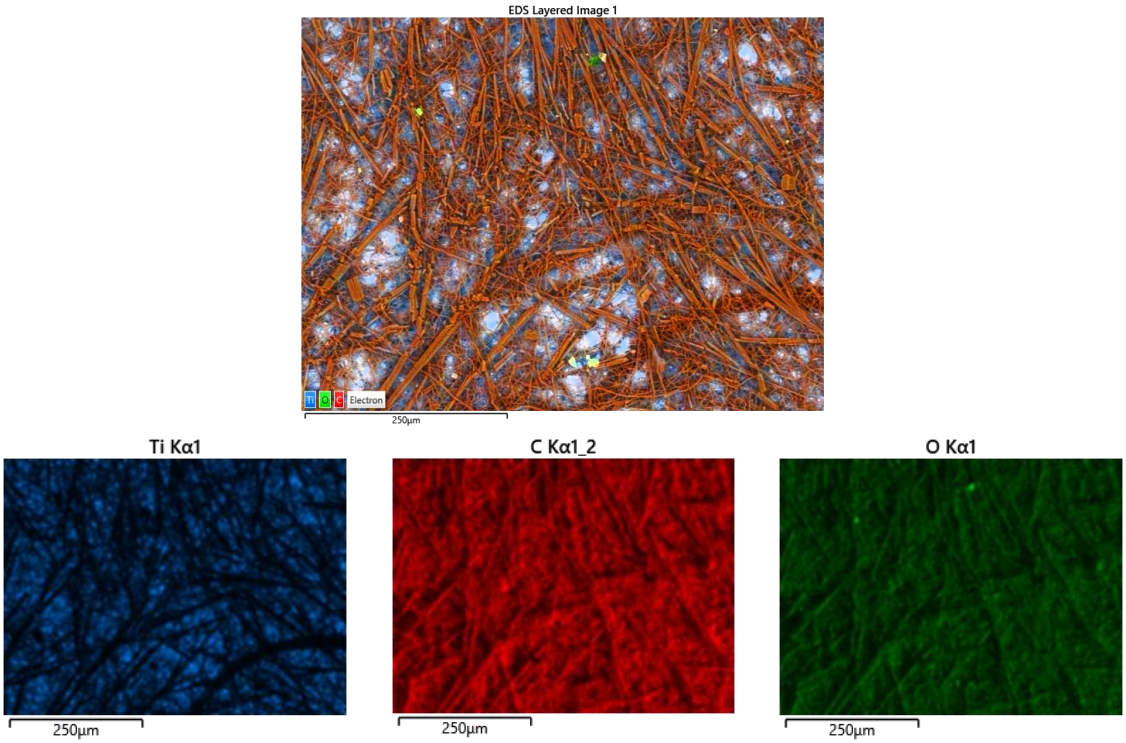

Figure 6.
Elemental Mapping of Metronidazole-Loaded PCL Nanowires via EDS Overlay

The uniform distribution of carbon and oxygen confirms the presence of PCL throughout the sample and suggests a homogenous loading of the drug within the PCL matrix.

In the Figure 7, the EDX analysis provides a comprehensive elemental composition of the PCL nanofibers loaded with tetracycline. The elemental composition is dominated by carbon (38.6 wt%, σ = 0.1) and oxygen (33.9 wt%, σ = 0.1), reflecting the organic nature of PCL and the presence of tetracycline. The reduction in carbon percentage is consistent with the introduction of tetracycline HCl, which dilutes the overall carbon concentration due to its composition that includes other atoms like nitrogen, oxygen and chlorine. A notable peak for chlorine (Cl) at 2.6 keV (1.9 wt%, σ = 0.0) serves as a marker for tetracycline, confirming its successful incorporation into the nanofibers. The titanium peaks, corresponding to the substrate, further contribute to the structural integrity and potential antimicrobial activity of the composite material.

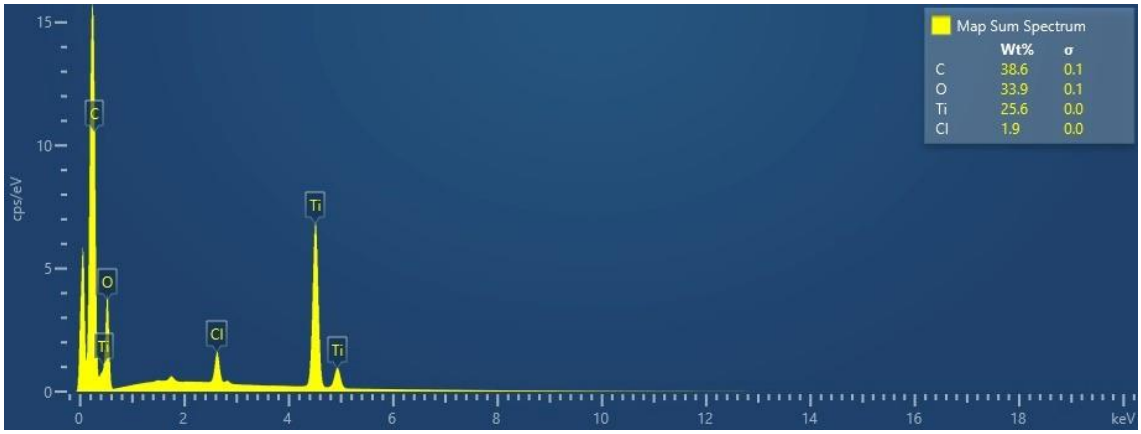

Figure 7.
EDX Spectrum Analysis of Tetracycline loaded on PCL Nanofibers

The EDX spectrum image visualizes the elemental composition through characteristic peaks at different energy levels (keV). The carbon peak appears prominently at around 0.3 keV, indicating the dominance of carbon in the sample due to the PCL nanofibers. The oxygen peak is noticeable at approximately 0.5 keV, supporting

the substantial oxygen content found in PCL and possibly indicating the presence of tetracycline. Titanium peaks are seen around 4.5 keV, showing signals of titanium in the sample, consistent with the composition of the substrate. The chlorine peak appears near 2.6 keV, although smaller in magnitude compared to carbon and oxygen, confirming the presence of tetracycline on the nanofibers.

The EDX analysis verifies the successful fabrication of tetracycline-loaded PCL nanofibers. The significant peaks for carbon and oxygen validate the presence of PCL, while the chlorine peak confirms the loading of tetracycline.

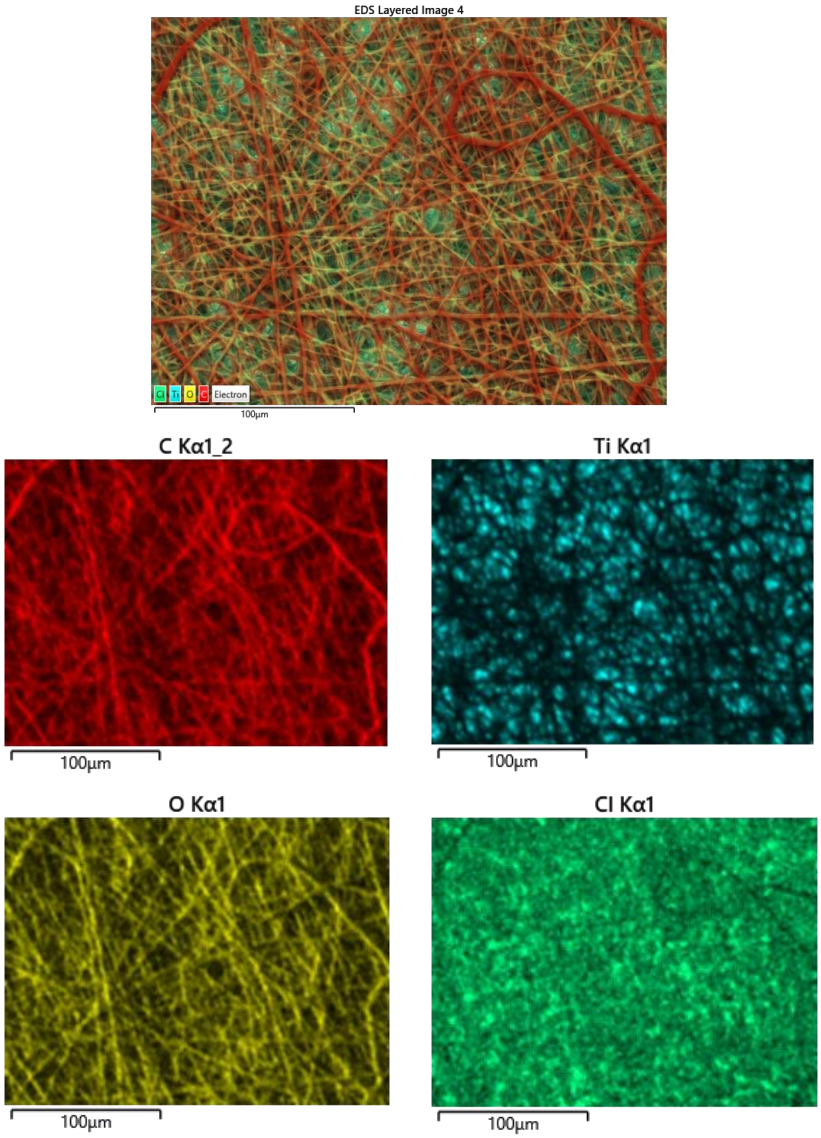

Figure 8.
Elemental Mapping of Tetracycline-Loaded PCL Nanowires via EDS Overlay

Figure 8 is an Energy Dispersive X-ray Spectroscopy (EDS) layered image that overlays the distribution of different elements across the sample. The colours represent the following: Red: corresponds to carbon (C), representing the PCL nanowires; Yellow: represents oxygen (O), which is present in both the PCL matrix and potentially the tetracycline; Green: corresponds to chlorine (Cl), which is a key element in tetracycline, indicating the drug distribution within the nanowires; Blue: represents titanium (Ti), showing the underlying Ti substrate.

The overlap of red and green colours indicates where C and Cl coexist, suggesting good integration of the tetracycline into the PCL nanowires.

The layered image shows a comprehensive view of how the elements are distributed.

Carbon map (C Kα1_2) shows the distribution of carbon across the sample, represented by the red colour. It indicates the location of the PCL nanowires, which form the bulk of the fibrous network. The dense, wide-spread red areas confirm that the PCL nanowires are

uniformly distributed, providing a consistent matrix for tetracycline loading.

Titanium Map (Ti Kα1), represented by the blue colour, shows where the support is located, typically under the PCL nanowire mat. The blue spots suggest areas where the titanium substrate is either exposed or close to the surface, indicating its role as a support for the nanowires.

Oxygen map (O Kα1) shows the distribution of oxygen, represented by the yellow colour. Oxygen is expected in both the PCL nanowires and possibly in tetracycline. The yellow areas confirm the presence of both the PCL matrix (due to ester groups) and the tetracycline (due to oxygen atoms in the molecule).

Chlorine map (Cl Kα1) shows the distribution of chlorine, represented by the green colour. The green areas confirm the presence of tetracycline within the nanowires, indicating successful drug loading. The distribution suggests that tetracycline is integrated into the PCL structure, likely dispersed throughout the nanowires.

The images collectively demonstrate the successful loading of tetracycline into PCL nanowires deposited on a titanium substrate. The EDS layered image shows the spatial relationship between the PCL matrix, the tetracycline and the titanium support. The individual elemental maps provide further detail on the distribution of key elements (C, Ti, O, Cl), confirming that the tetracycline is well-distributed within the PCL nanowires, with the titanium substrate providing structural support.

Fourier-transform infrared spectroscopy (FTIR)

Fourier-transform infrared (FTIR) spectroscopy was employed to confirm the successful incorporation of tetracycline (TC) and metronidazole (MTZ) into Zr-PCL composites.

SEM images of the PCL nanowires reveal a consistent and uniform structure, providing a solid foundation for the incorporation of active pharmaceutical agents. This structural integrity is further supported by FTIR analysis, which confirms the presence of tetracycline and metronidazole on the nanowires. The combination of these detailed structural insights from SEM with the chemical validation from FTIR shows the successful functionalization of the PCL nanowires with the antimicrobial agents, enhancing their potential effectiveness in biomedical applications.

Therefore, the Zr spectrum exhibited characteristic peaks at 3400 cm^{-1}, 1640 cm^{-1} and 1000 - 1100 cm^{-1}, consistent with previous studies on zirconium-based materials [55, 56]. The Zr-PCL spectrum showed additional peaks at 2944 cm^{-1} and 2866 cm^{-1} (C-H stretching), 1724 cm^{-1} (C=O stretching) and 1164 cm^{-1} (C-O stretching), indicative of PCL integration [57, 58]. The Zr-PCL-TC composite spectrum revealed distinctive peaks at 3301 cm^{-1} (O-H stretching), 1647 cm^{-1} (C=O stretching) and 1457 cm^{-1} (C-H bending), confirming the presence of tetracycline [59, 60] (Figure 9).

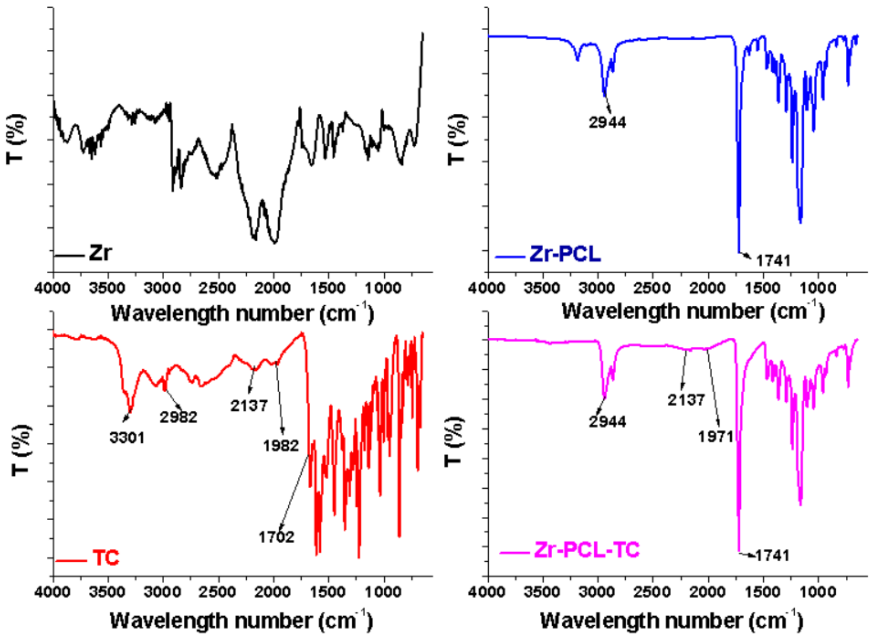

Figure 9.
FTIR spectrum for Zr-PCL-MTZ

In contrast, the Zr-PCL-MTZ spectrum displayed characteristic peaks at 3097 cm^{-1}, 1535 cm^{-1} (NO_2 asymmetric stretching) and 1369 cm^{-1} (NO_2 symmetric stretching), validating the incorporation of metronidazole [61, 62] (Figure 10). The presence of these drug-specific peaks, alongside the characteristic signals of

Zr and PCL, provides strong evidence for the successful synthesis of drug-loaded zirconium-based composites without significant chemical alterations to the individual components. This spectral analysis aligns with previous research on drug-loaded polymer composites [63], demonstrating the versatility of the Zr-PCL matrix in accommodating different therapeutic agents. The preservation of key functional groups from both the matrix materials and the drugs suggests that the composites maintain their intended chemical properties, which is crucial for their potential biomedical applications. These results not only confirm the effective integration of TC and MTZ into the Zr-PCL matrix but also highlight the potential of these composites for targeted drug delivery systems or antimicrobial materials. The distinct spectral fingerprints of each composite provide a reliable method for quality control and batch-to-batch consistency in future large-scale production. Furthermore, the successful incorporation of drugs with different hydrophilicity, such as MTZ or TC, into the Zr-PCL matrix demonstrates the broad applicability of this composite system, opening avenues for the development of multifunctional biomaterials with tailored drug release profiles [63].

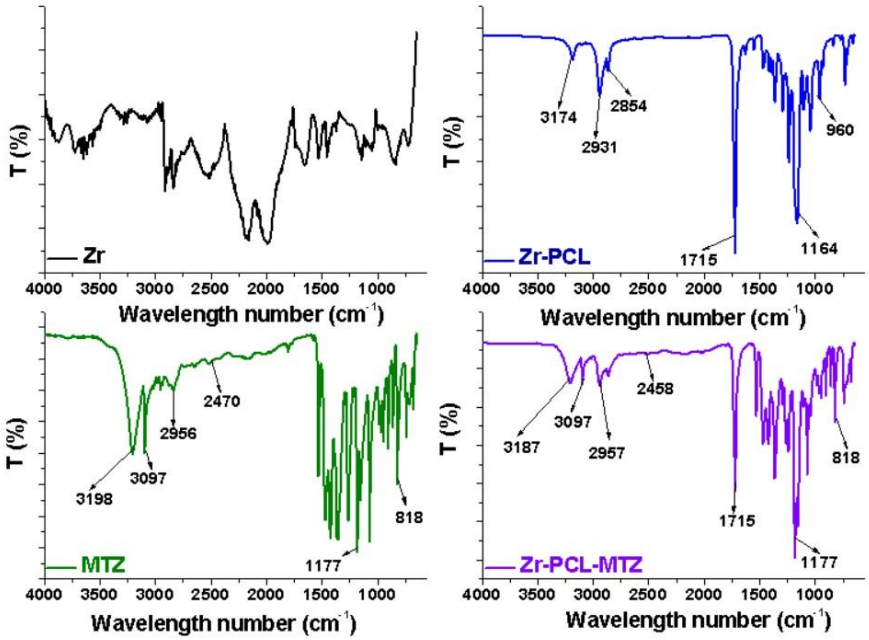

Figure 10.
FTIR spectrum for Zr-PCL-MTZ

Contact Angle

The contact angle measurements of the PCL nanowires provide insight into their surface wettability, which is influenced by both their structural and chemical properties. SEM images reveal a uniform and well-defined surface morphology, which can contribute to consistent contact angle values across the nanowires. The FTIR analysis further complements this by confirming the presence of tetracycline and metronidazole on the nanowires, which may modify surface chemistry and, consequently, the contact angle. The interplay between the nanowires' morphology, as observed in SEM, and their chemical composition, as indicated by FTIR, plays a crucial role in determining their surface wettability, which is a key factor in their interaction with biological environments and their potential effectiveness in antimicrobial applications.

Contact angle measurements are pivotal in understanding the wettability and hydrophobicity of material surfaces, which directly influence their antibacterial capabilities. In our study, we evaluated the contact angles of four different samples: pure zirconium (Zr), zirconium covered with PCL wires (Zr-PCL), tetracycline loaded PCL nanowires on zirconium substrate (Zr-PCL-TC) and metronidazole loaded PCL nanowires on zirconium substrate (Zr-PCL-MTZ) (Figure 11).

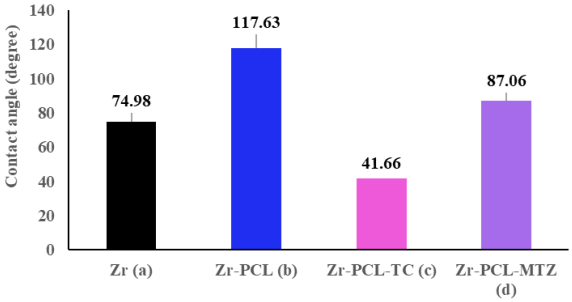

Figure 11.
Contact angle measurements for the sample (a) uncoated Zr, (b) Zr-PCL, (c) Zr-PCL-TC and (d) Zr-PCL-MTZ

The pure Zr sample exhibited a contact angle of 74.98°, indicating a moderately hydrophilic surface. While pure zirconium possesses some inherent antibacterial properties, its effectiveness is relatively limited. The Zr-PCL sample had a contact angle of 117.63°, demonstrating a highly hydrophobic surface. This high hydrophobicity may reduce initial bacterial adhesion; however, since PCL lacks intrinsic antibacterial properties, this configuration is likely the least effective in preventing bacterial growth.

The Zr-PCL-TC sample showed a significant decrease in the contact angle to 41.66°, indicating a highly hydrophilic surface. The addition of tetracycline, a potent antibiotic, coupled with the enhanced wettability, suggests a substantial improvement in antibacterial activity. The hydrophilic nature of the surface promotes better drug release and interaction with bacterial cells, thereby enhancing overall antibacterial efficacy.

The Zr-PCL-MTZ sample exhibited a contact angle of 87.06°, indicating a slightly hydrophilic surface. Metronidazole, another effective antibiotic, contributes to the antibacterial properties of this sample. Although less hydrophilic compared to Zr-PCL-TC, the moderate hydrophilicity of Zr-PCL-MTZ facilitates some level of drug release and bacterial interaction, resulting in moderate antibacterial activity.

In summary, the Zr-PCL-TC combination displayed the highest antibacterial activity due to the synergistic effects of the highly hydrophilic surface and the presence of tetracycline. The Zr-PCL-MTZ configuration showed moderate antibacterial activity, while pure Zr and Zr-PCL demonstrated the least antibacterial effectiveness, with Zr-PCL being the lowest due to its hydrophobic nature and lack of inherent antibacterial agents.

In vitro release kinetics

Each zirconium plate coated with PCL fibres contains 1.398 mg ± 0.117 mg of metronidazole, highlighting an efficient incorporation of this antibiotic into the fibre structure. In the case of tetracycline, the amount loaded into the PCL fibres is 0.244 mg ± 0.0163 mg *per* plate. The differences in the quantity of antibiotic incorporated may be influenced by factors such as the affinity of the PCL fibres for each active substance, the interactions between PCL and the Zr substrate, as well as the specific parameters of the fibre deposition process onto the substrate.

The *in vitro* release profiles of metronidazole (MTZ) and tetracycline (TC) from the Zr-PCL-TC-MTZ and Zr-PCL-TC samples were investigated over a period of 360 hours.

The release profile of metronidazole from the Zr-PCL-MTZ sample shows a typical biphasic release pattern (Figure 12a), characterised by an initial burst release followed by a slower, sustained release phase, with just under 80% of the total drug amount released within 15 days. The initial rapid release is likely due to the immediate dissolution of metronidazole particles present on or near the surface of the PCL nanofibers, which are readily accessible to the surrounding medium. This burst release phase is advantageous in achieving an immediate therapeutic effect, especially in acute infection scenarios [64]. Following this burst, the release rate gradually decreases as the drug diffuses from the deeper layers of the polymer matrix. This sustained release phase suggests that the metronidazole is effectively encapsulated within the nanofibers, allowing for a controlled release over an extended period.

Similar to metronidazole, tetracycline exhibits an initial burst release followed by a more gradual, sustained release (Figure 12b). However, it is important to note that after 168 hours slight degradation of tetracycline in the dissolution medium was observed, as indicated by the chromatographic analysis, interfering with the experiments by underestimating the total amount of tetracycline released from the fibres. For this reason, modelling of tetracycline release kinetics was performed only up to 168 hours.

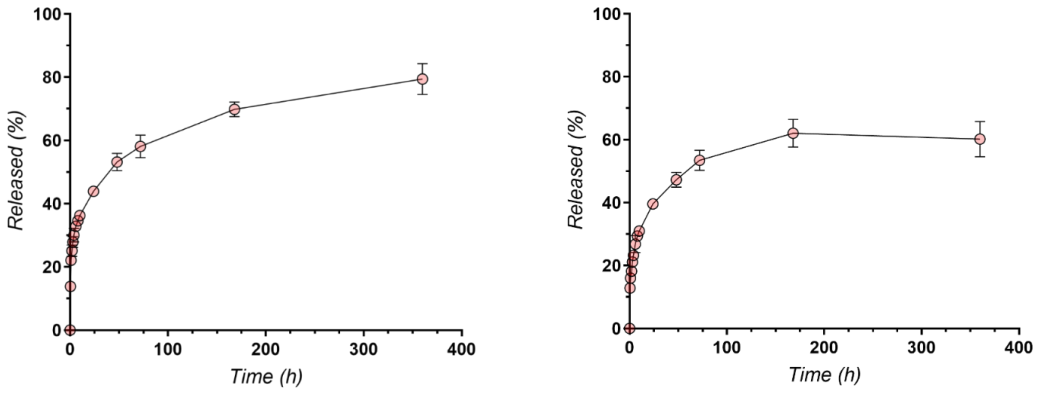

Figure 12.
Release profile of (a) metronidazole and (b) tetracycline (n = 3)

The experimental release data were fitted to several diffusion-based mathematical models to elucidate the underlying mechanisms governing drug release. The results of these fittings are graphically represented in Figure 13 and Figure 14, while the corresponding kinetic parameters and correlation coefficients are detailed in Table I.

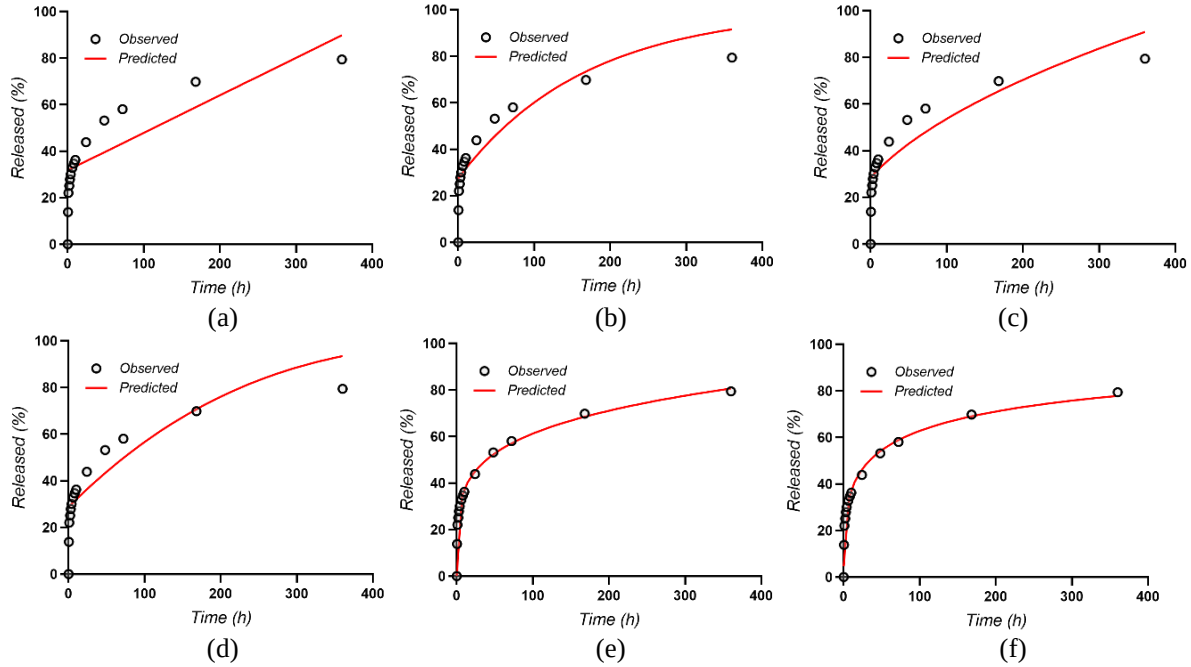

Figure 13.
Kinetic models of MTZ release (a) Zero order; (b) First order; (c) Higuchi, (d) Hixson-Crowell, (e) Korsmeyer-Peppas; (f) Weibull

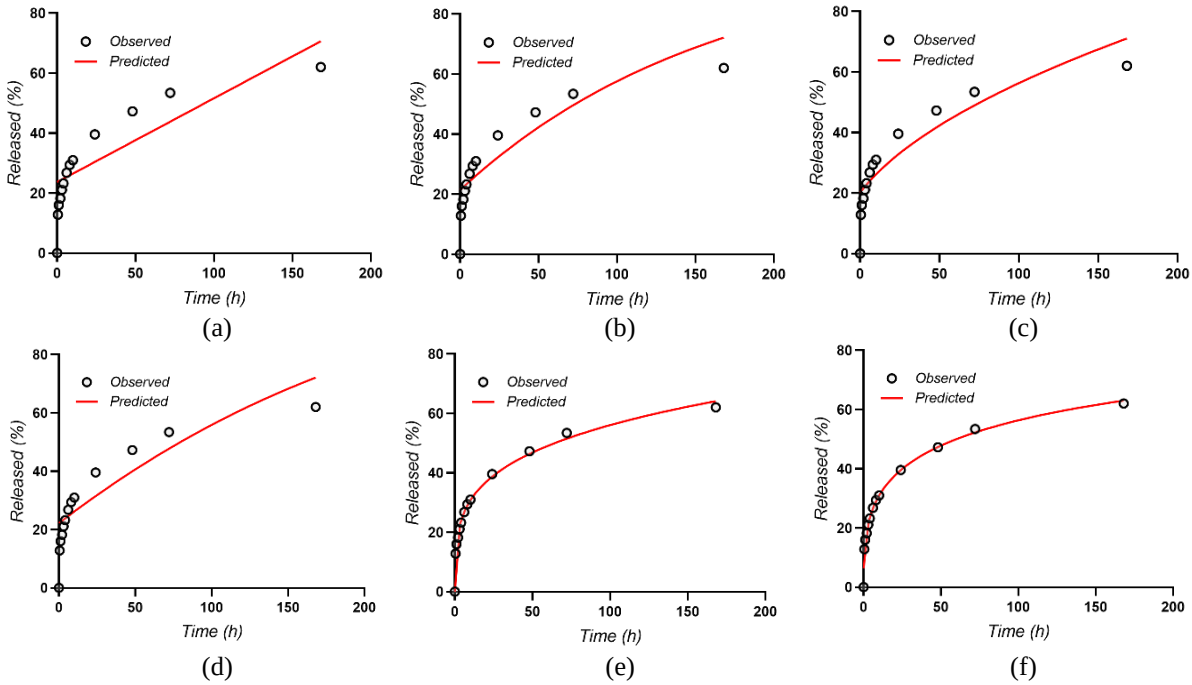

Figure 14.
Kinetic models of TC release (a) Zero order; (b) First order; (c) Higuchi, (d) Hixson-Crowell, (e) Korsmeyer-Peppas; (f) Weibull

Table I

Kinetic parameters and correlation coefficients (R^2) for the release of MTZ and TC from Zr-PCL Nanofibers fitted to various mathematical models

Model	Parameter	Sample	
		Zr-PCL-MTZ	Zr-PCL-TC
Zero Order	k_0	0.161	0.280
	R^2	0.7094	0.7451
First Order	k_1	0.006	0.006
	R^2	0.8622	0.8430
Higuchi	k_H	4.551	5.257
	R^2	0.8199	0.8669
Hixson- Crowell	k_{HC}	0.001	0.002
	R^2	0.8180	0.8113
Korsmeyer-Peppas	k_{KP}	22.854	17.056
	n	0.214	0.258
	R^2	0.9973	0.9984
Weibull	α	4.591	6.087
	β	0.329	0.352
	R^2	0.9935	0.9961

Among the models tested, the Korsmeyer-Peppas model emerged as the most accurate for both MTZ and TC, as evidenced by the exceptionally high correlation coefficients (R^2 = 0.9973 for MTZ and 0.9984 for TC). The values of the release exponent n, 0.214 for MTZ and 0.258 for TC, indicate a Fickian diffusion mechanism, suggesting that drug release is predominantly governed by diffusion through the polymer matrix rather than by erosion or degradation processes [65]. The Weibull model also provided a strong fit (R^2 = 0.9935 for MTZ and 0.9961 for TC), supporting the complexity of the release mechanism. The shape parameters (α and β) obtained from the Weibull model further reinforce the notion that the drug release profile is influenced by a combination of diffusion and polymer relaxation dynamics. The excellent fit to the Weibull model suggests that while diffusion is the primary release mechanism, other factors such as polymer relaxation or structural changes in the matrix may play a secondary role [66].

In conclusion, the Zr-PCL nanofibers demonstrate a promising controlled release profile for both metronidazole and tetracycline, primarily driven by diffusion through the polymer matrix. The consistency and reliability of the Korsmeyer-Peppas model's fit underscore the potential of these nanofibers for long-term drug delivery applications, particularly in the management of chronic infections where sustained antimicrobial activity is required.

Antibacterial effect

According to Figure 15 and Figure 16, no inhibition zone is observed around the control plate (Zr), indicating that the Zr substrate alone does not have an anti-microbial effect against the selected microorganisms. The plates containing tetracycline inhibited the growth of both Gram-negative bacilli (*E. coli*) and Gram-positive cocci (*S. aureus*), demonstrating a clear anti-microbial effect against these microorganisms (Table II). Similar to the control, there is no visible inhibition zone around the Zr-PCL-MTZ, indicating that the metronidazole does not inhibit the growth of the selected microorganisms. This aligns with the known properties of metronidazole, which is primarily effective against anaerobic bacteria, not aerobic bacteria like *E. coli* or *S. aureus*. It is more suitable for treating infections where anaerobic bacteria are present and where oxygen levels are low.

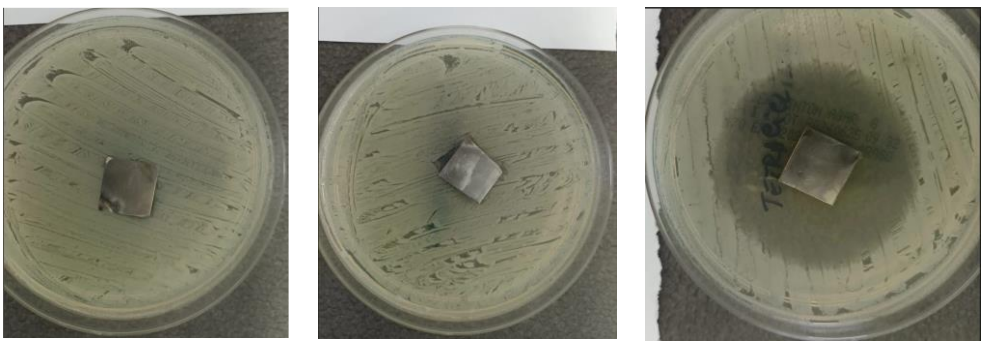

(a) (b) (c)

Figure 15.

Antimicrobial activity against *Staphylococcus aureus* for (a) Zr, (b) Zr-PCL-MTZ and (c) Zr-PCL-TC

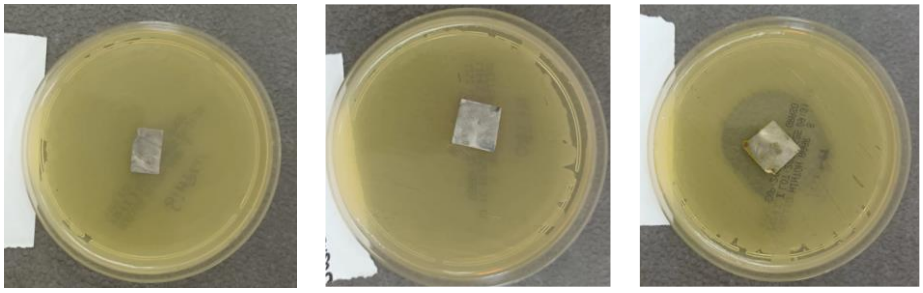

(a) (b) (c)

Figure 16.
Antimicrobial activity against *Escherichia coli* for **(**a) Zr, (b) Zr-PCL-MTZ and (c) Zr-PCL-TC

Table II
Diameter of inhibition zone of bacteria, determined by Zr-PCL-TC

Bacterium	Inhibition Zone Diameter
Staphylococcus aureus	52 mm
Escherichia coli	43 mm

According to standardised guidelines, such as those established by the CLSI (Clinical and Laboratory Standards Institute) [67], bacteria are considered "susceptible" to an antibiotic if the inhibition zone is larger than a certain minimum diameter, specific to each type of bacterium. For *Staphylococcus aureus*, the susceptibility threshold is defined by an inhibition zone diameter of 19 mm or greater, halo diameter being calculated for a disc concentration of 30 µg tetracycline. The result obtained shows an inhibition zone of 52 mm, which is significantly larger than this threshold, indicating that *Staphylococcus aureus* is highly susceptible to the sample containing tetracycline. For *Escherichia coli*, the susceptibility threshold has a minimum inhibition zone diameter of 15 mm. The result obtained, an inhibition zone of 43 mm, is also much larger than this threshold, indicating that *E. coli* is highly susceptible to the sample containing tetracycline.
Bacterial susceptibility to an antibiotic reflects its effectiveness against them. The larger the inhibition zone, the more effective the antibiotic is at the concentration used in inhibiting bacterial growth. In this case, *Staphylococcus aureus* and *Escherichia coli* exhibited considerable inhibition zones, suggesting that tetracycline is highly effective against these bacteria. This means that, in treating an infection caused by these bacteria, tetracycline would be an excellent choice, as the bacteria are highly susceptible to this antibiotic.

Conclusions

The study demonstrated that Zr-PCL-MTZ and Zr-PCL-TC exhibit favourable morphological and chemical properties for use as controlled drug release systems. SEM analysis revealed a uniform distribution of the nanofibers, which, according to EDX and FTIR, ensures efficient loading and integration of the antibiotics, enhancing their antimicrobial activity. Contact angle measurements indicated an increase in surface hydrophilicity, a factor that contributes to the prevention of bacterial colonization and suggest good surface interaction with biological environments, while the antibiotic release profile confirmed sustained and efficient release, essential for maintaining long-term antibacterial activity. The antibacterial efficiency was validated through tests against *Escherichia coli* and *Staphylococcus aureus*, thus demonstrating the potential of these structures in preventing infections associated with medical devices. The results indicate a strong correlation between the morphological structure of the nanofibers, surface properties and antibacterial performance, supporting the use of this technology in biomedical applications.
The results obtained from the antibiogram indicate that both *Staphylococcus aureus* and *Escherichia coli* are highly sensitive to tetracycline, suggesting that this antibiotic would be extremely effective in treating infections caused by these bacteria.

Conflict of interest

The authors declare no conflict of interest.

References

1. Ramos AP, Cruz MA, Tovani CB, Ciancaglini P, Biomedical applications of nanotechnology. *Biophys Rev.*, 2017; 9(2): 79-89.
2. Pokrajac L, Abbas A, Chrzanowski W, Dias GM, Eggleton BJ, Maguire S, Maine E, Malloy T, Nathwani J, Nazar L, Nanotechnology for a sustainable future: Addressing global challenges with the international network4sustainable nanotechnology. *ACS Publications*, 2021; 15(12): 18608-18623.
3. Mohapatra SS, Frisina RD, Mohapatra S, Sneed KB, Markoutsa E, Wang T, Dutta R, Damnjanovic R, Phan MH, Denmark DJ, Advances in translational nanotechnology: challenges and opportunities. *Appl Sci (Basel)*, 2020; 10(14): 4881.
4. Hsu CY, Rheima AM, sabri Abbas Z, Faryad MU, Kadhim MM, Altimari US, Dawood AH, Abed ZT, Radhi RS, Jaber AS, Nanowires properties and applications: a review study. *South African J Chem Engine.*, 2023; 46: 286-311.

5. Park S, Saravanakumar K, Zhang X, Jeong MS, Wang MH, Tetracycline-loaded zirconium oxide nanoparticles synthesized by *Lactobacillus rhamnosus* effectively eradicate bacterial biofilms. *Inorganic Chemistry Communications*, 2022; 145: 109978.
6. Oliveira A, Araújo A, Rodrigues LC, Silva CS, Reis RL, Neves NM, Leão P, Martins A, Metronidazole Delivery Nanosystem Able To Reduce the Pathogenicity of Bacteria in Colorectal Infection. *Biomacromolecules*, 2022; 23(6): 2415-2427.
7. Shende P, Basarkar V, Recent trends and advances in microbe-based drug delivery systems. *DARU J Pharmaceut Sci*., 2019; 27: 799-809.
8. Tan Y, Ma S, Leonhard M, Moser D, Haselmann GM, Wang J, Eder D, Schneider-Stickler B, Enhancing antibiofilm activity with functional chitosan nanoparticles targeting biofilm cells and biofilm matrix. *Carbohydrate Polymers*, 2018; 200: 35-42.
9. Khan M, Shaik MR, Khan ST, Adil SF, Kuniyil M, Khan M, Al-Warthan AA, Siddiqui MRH, Nawaz Tahir M, Enhanced antimicrobial activity of biofunctionalised zirconia nanoparticles. *ACS Omega*, 2020; 5(4): 1987-1996.
10. Uddin TM, Chakraborty AJ, Khusro A, Zidan BRM, Mitra S, Emran TB, Dhama K, Ripon MKH, Gajdács M, Sahibzada MUK, Antibiotic resistance in microbes: History, mechanisms, therapeutic strategies and future prospects. *J Infect Public Health*, 2021; 14(12): 1750-1766.
11. Ezike TC, Okpala US, Onoja UL, Nwike CP, Ezeako EC, Okpara OJ, Okoroafor CC, Eze SC, Kalu OL, Odoh EC, Advances in drug delivery systems, challenges and future directions. *Heliyon*, 2023; 9(6): e17488.
12. Nazli A, He DL, Liao D, Khan MZI, Huang C, He Y, Strategies and progresses for enhancing targeted antibiotic delivery. *Adv Drug Deliv Rev.*, 2022; 189: 114502.
13. Aparicio-Blanco J, Vishwakarma N, Lehr CM, Prestidge CA, Thomas N, Roberts RJ, Thorn CR, Melero A, Antibiotic resistance and tolerance: What can drug delivery do against this global threat?. *Drug Deliv Translat Res.*, 2024; 14(6): 1725-1734.
14. Alibrahim KA, FTIR, ^{1}H NMR, TGA, TEM and biological studies on the new synthesized nano zirconium(IV) captopril hypertension drug complex. *Farmacia*., 2022; 70(1): 133-137.
15. Zupančič Š, Potrč T, Baumgartner S, Kocbek P, Kristl J, Formulation and evaluation of chitosan/polyethylene oxide nanofibers loaded with metronidazole for local infections. *Eur J Pharmaceut Sci.*, 2016; 95: 152-160.
16. Lin H, Yin C, Mo A, Zirconia based dental biomaterials: structure, mechanical properties, biocompatibility, surface modification, and applications as implant. *Front Dental Med.*, 2021; 2: 689198.
17. Han MK, Advances and challenges in zirconia-based materials for dental applications. *J Korean Ceramic Soc.*, 2024: 1-17.
18. Singh PV, Reche A, Paul P, Agarwal S, Zirconia Facts and Perspectives for Biomaterials in Dental Implantology. *Cureus*, 2023; 15(10): e46828.
19. Jangra SL, Stalin K, Dilbaghi N, Kumar S, Tawale J, Singh SP, Pasricha R, Antimicrobial activity of zirconia (ZrO_2) nanoparticles and zirconium complexes. *J Nanosci Nanotechnol*., 2012; 12(9): 7105-7112.
20. Bannunah AM, Biomedical applications of zirconia-based nanomaterials: challenges and future perspectives. *Molecules*, 2023; 28(14): 5428.
21. Tabassum N, Kumar D, Verma D, Bohara RA, Singh M, Zirconium oxide (ZrO_2) nanoparticles from anti-bacterial activity to cytotoxicity: A next-generation of multifunctional nanoparticles. *Materials Today Communications*, 2021; 26: 102156.
22. Algabar FAA, Ahmed DS, Abbod LS, Al-Obaidi MA, Antibacterial Synergy: Assessing the Impact of Nano Zirconium Oxide Particles in Combination with Selected Antibiotics on *Escherichia coli* and *Klebsiella pneumoniae* Isolates from Urinary Tract Infections. *Ind J Microbiol*., 2024: 1-9.
23. Radu RD, Drăgănescu D, Present and future of ZrO_2 nanostructure as reservoir for Drug loading and release. *Coatings*, 2023; 13(7): 1273.
24. Leonetti B, Perin A, Ambrosi EK, Sponchia G, Sgarbossa P, Castellin A, Riello P, Scarso A, Mesoporous zirconia nanoparticles as drug delivery systems: Drug loading, stability and release. *J Drug Deliv Sci Technol*., 2021; 61: 102189.
25. Al-Awsi G, Alameri A, Al-Dhalimy A, Gabr G, Kianfar E, Application of nano-antibiotics in the diagnosis and treatment of infectious diseases. *Brazilian J Biol.*, 2023; 84: e264946.
26. Brammer KS, Choi C, Oh S, Cobb CJ, Connelly LS, Loya M, Kong SD, Jin S, Antibiofouling, sustained antibiotic release by Si nanowire templates. *Nano Lett.*, 2009; 9(10): 3570-3574.
27. Chopra I, Roberts M, Tetracycline antibiotics: mode of action, applications, molecular biology, and epidemiology of bacterial resistance. *Microbiol Mol Biol Rev.*, 2001; 65(2): 232-260.
28. Shutter MC, Akhondi H, Tetracycline. 2019 In: StatPearls [Internet]. Treasure Island (FL): StatPearls Publishing; 2024 Jan. 2023 Jun 5.
29. Weir CB, Le JK, Metronidazole. 2019. In: StatPearls [Internet]. Treasure Island (FL): StatPearls Publishing; 2024 Jan. 2023 Jun 26.
30. Kumar G, Chaudhary K, Mogha NK, Kant A, Masram DT, Extended release of metronidazole drug using chitosan/graphene oxide bionanocomposite beads as the drug carrier. *ACS Omega*, 2021; 6(31): 20433-20444.
31. Dingsdag SA, Hunter N, Metronidazole: an update on metabolism, structure–cytotoxicity and resistance mechanisms. *J Antimicrob Chemother.*, 2018; 73(2): 265-279.
32. Skwarczynski M, Bashiri S, Yuan Y, Ziora ZM, Nabil O, Masuda K, Khongkow M, Rimsueb N, Cabral H, Ruktanonchai U, Antimicrobial activity enhancers: Towards smart delivery of antimicrobial agents. *Antibiotics*, 2022; 11(3): 412.
33. Rasouli R, Barhoum A, Advances in nanofibers for antimicrobial drug delivery, in Handbook of nanofibers. Ed. Springer. 2019; 733-774.
34. Khanzada H, Kumpikaitė E, Anti-bacterial nanofibers and their biomedical applications–a review. *J Textile Institute*, 2024; 2024: 1-19.
35. Adepu S, Ramakrishna S, Controlled drug delivery systems: current status and future directions. *Molecules*, 2021; 26(19): 5905.

36. Mim JJ, Hasan M, Chowdhury MS, Ghosh J, Mobarak MH, Khanom F, Hossain N, A comprehensive review on the biomedical frontiers of nanowire applications. *Heliyon*, 2024.
37. Geng Z, Cao Z, Liu J, Recent advances in targeted antibacterial therapy basing on nanomaterials. in *Exploration*. 2023. Wiley Online Library.
38. Shaw Z, Kuriakose S, Cheeseman S, Dickey MD, Genzer J, Christofferson AJ, Crawford RJ, McConville CF, Chapman J, Truong VK, Antipathogenic properties and applications of low-dimensional materials. *Nature Communications*, 2021; 12(1): 3897.
39. Makabenta JMV, Nabawy A, Li CH, Schmidt-Malan S, Patel R, Rotello VM, Nanomaterial-based therapeutics for antibiotic-resistant bacterial infections. *Nature Rev Microbiol.*, 2021; 19(1): 23-36.
40. Bahammam HA, Bahammam LA, Baghdadi AM, Saddiq A, Algamal Y, Antimicrobial Activity of Nanozirconium Oxide. *ACS Omega*, 2024; 9(2): 2945-2952.
41. Mohammadian F, Eatemadi A, Drug loading and delivery using nanofibers scaffolds. *Artif Cells Nanomed Biotechnol.*, 2017; 45(5): 881-888.
42. Hamdan N, Yamin A, Hamid S, Khodir W, Guarino V, Functionalised antimicrobial nanofibers: design criteria and recent advances. *J Funct Biomater.*, 2021; 12(4): 59.
43. Maliszewska I, Czapka T, Electrospun polymer nanofibers with antimicrobial activity. *Polymers*, 2022; 14(9): 1661.
44. Zaborowska M, Smok W, Tański T, Electrospinning synthesis and characterization of zirconia nanofibers annealed at different temperatures. *Appl Surf Sci.*, 2023; 615: 156342.
45. Ridwan M, Prastya ME, Fadilah C, Ariani N, Al Muttaqii M, Andreani AS, Improved antimicrobial activities of biphasic titania nanowires against gram-negative and gram-positive bacteria. *Kuwait J Sci.*, 2024: 100256.
46. Srithep Y, Akkaprasa T, Pholharn D, Morris J, Liu SJ, Patrojanasophon P, Ngawhirunpat T, Metronidazole-loaded polylactide stereocomplex electrospun nanofiber mats for treatment of periodontal disease. *J Drug Deliv Sci Technol.*, 2021; 64: 102582.
47. Mirzaeei S, Mansurian M, Asare-Addo K, Nokhodchi A, Metronidazole-and amoxicillin-loaded PLGA and PCL nanofibers as potential drug delivery systems for the treatment of periodontitis: *in vitro* and *in vivo* evaluations. *Biomedicines*, 2021; 9(8): 975.
48. e Silva GLG, de Bustamante MSdS, Dias ML, Costa AM, Rossi AM, dos Santos Matos AP, Santos-Oliveira R, Ricci-Junior E, Antibiotics-loaded nanofibers fabricated by electrospinning for the treatment of bone infections. *Arabian J Chem.*, 2023; 16(1): 104392.
49. Adeniji OO, Nontongana N, Okoh JC, Okoh AI, The potential of antibiotics and nanomaterial combinations as therapeutic strategies in the management of multidrug-resistant infections: a review. *Int J Mol Sci.*, 2022; 23(23): 15038.
50. Nandhini J, Karthikeyan E, Rajeshkumar S, Nanomaterials for wound healing: Current status and futuristic frontier. *Biomed Technol.*, 2024; 6: 26-45.
51. Musuc AM, Anuta V, Atkinson I, Sarbu I, Popa VT, Munteanu C, Mircioiu C, Ozon EA, Nitulescu GM, Mitu MA, Formulation of chewable tablets containing carbamazepine-β-cyclodextrin inclusion complex and f-melt disintegration excipient. The mathematical modeling of the release kinetics of carbamazepine. *Pharmaceutics*, 2021; 13(6): 915.
52. Quest Calculate™ PBS (Phosphate Buffered Saline) (1X, pH 7.4) Preparation and Recipe. www.aatbio.com/resources/buffer-preparations-and-recipes/pbs-phosphate-buffered-saline.
53. Zhang L, Wang Y, Jia L, Bi N, Bie H, Chen X, Zhang C, Xu J, Ultrasensitive and visual detection of tetracycline based on dual-recognition units constructed multicolor fluorescent nano-probe. *J Hazard Mat.*, 2021; 409: 124935.
54. Shaheed D, Bader Q, Abbas A, Spectrophotometric determination of metronidazole benzoate in pharmaceutical dosage forms. *Int J Pharm Res.*, 2020; 12: 3526-3532.
55. Munir M, Sarmini E, Saptiama I, Billah A. Characterization of Zirconium-Based Material (ZBM) Synthetised by Gradual Drying for Molybdenum-99 (99Mo) Adsorbent. in *IOP Conference Series: Materials Science and Engineering*. 2019. *IOP Publishing*.
56. Efaw CM, Vandegrift JL, Reynolds M, Jaques BJ, Hu H, Xiong H, Hurley MF, Characterization of zirconium oxides part II: New insights on the growth of zirconia revealed through complementary high-resolution mapping techniques. *Corrosion Sci.*, 2020; 167: 108491.
57. Phillipson K, Hay J, Jenkins M, Thermal analysis FTIR spectroscopy of poly (ε-caprolactone). *Thermochimica Acta*, 2014; 595: 74-82.
58. Benkaddour A, Jradi K, Robert S, Daneault C, Grafting of polycaprolactone on oxidised nanocelluloses by click chemistry. *Nanomaterials*, 2013; 3(1): 141-157.
59. Bittner B, Mäder K, Kroll C, Borchert HH, Kissel T, Tetracycline-HCl-loaded poly (DL-lactide-co-glycolide) microspheres prepared by a spray drying technique: influence of γ-irradiation on radical formation and polymer degradation. *J Control Release*, 1999; 59(1): 23-32.
60. Turan CU, Metin A, Guvenilir Y, Controlled release of tetracycline hydrochloride from poly (ω-pentadecalactone-co-ε-caprolactone)/gelatin nanofibers. *Eur J Pharmaceut Biopharmaceut.*, 2021; 162: 59-69.
61. Trivedi M, Patil S, Shettigar H, Bairwa K, Jana S, Spectroscopic characterization of biofield treated metronidazole and tinidazole. *Medicin Chem.*, 2015; 7(5): 340-344.
62. Naseem F, Shah SU, Rashid SA, Farid A, Almehmadi M, Alghamdi S, Metronidazole based floating bioadhesive drug delivery system for potential eradication of H. pylori: preparation and *in vitro* characterization. *Polymers*, 2022; 14(3): 519.
63. Tong X, Pan W, Su T, Zhang M, Dong W, Qi X, Recent advances in natural polymer-based drug delivery systems. *Reactive Functl Polym.*, 2020; 148: 104501.
64. Fierascu I, Fierascu IC, Dinu-Pirvu CE, Fierascu RC, Anuta V, Velescu BS, Jinga M, Jinga V, A short overview of recent developments on antimicrobial coatings based on phytosynthesized metal nanoparticles. *Coatings*, 2019; 9(12): 787.
65. Tudoroiu EE, Kaya MGA, Titorencu I, Dinu-Pîrvu CE, Marin MM, Roșca AM, Popa L, Anuța V, Antoniac A, Chelaru C, Design and evaluation of new wound

dressings based on collagen-cellulose derivatives. *Mater Design*, 2023; 236: 112469.

66. Mircioiu I, Anuta V, Purcaru SO, Radulescu F, Miron D, Dumitrescu IB, Ibrahim N, Mircioiu C, *In vitro* dissolution of poorly soluble drugs in the presence of surface-active agents-*in vivo* pharmacokinetics correlations. II. Nimesulide. *Farmacia*, 2013; 61(1): 88-102.
67. Global Standards for Antimicrobial Susceptibility Testing. 2024.